Research Article | Vol. 8, No. 12 | 1 Dec 2017 | BIOMEDICAL OPTICS EXPRESS 5533
Biomedical Optics EXPRESS

Three-dimensional side-view endomicroscope for tracking individual cells *in vivo*

XIYU DUAN,[1,4] HAIJUN LI,[1,4] FA WANG,[1] XUE LI,[1] KENN R. OLDHAM,[2] AND THOMAS D. WANG[1,2,3,*]

[1]*Department of Internal Medicine, Division of Gastroenterology, University of Michigan, Ann Arbor, MI 48109, USA*
[2]*Department of Mechanical Engineering, University of Michigan, Ann Arbor, MI 48109, USA*
[3]*Department of Biomedical Engineering, University of Michigan, Ann Arbor, MI 48109, USA*
[4]*These authors contributed equally to this work*
[*]*thomaswa@umich.edu*

Abstract: We demonstrate a side-view endomicroscope using a monolithic 3-axis scanner placed in the post-objective position that performs either tilt or piston motion to achieve either optical scan angles >10° or large vertical displacements, respectively. This configuration allows for scaling down of instrument dimensions for high maneuverability and accurate positioning in vivo. Images exceeded either 700 × 600 μm^2 in the horizontal plane or vertical depths of 200 μm. Resolution of 1.19 and 3.46 μm was obtained in the horizontal and oblique planes, respectively. Optical sections were collected from dysplastic colonic epithelium in vivo in mice that express tdTomato at 10 Hz to visualize individual cells.

OCIS codes: (170.6900) Three-dimensional microscopy; (120.5800) Scanners; (170.2520) Fluorescence microscopy.

References and links

1. L. W. Peterson and D. Artis, "Intestinal epithelial cells: regulators of barrier function and immune homeostasis," Nat. Rev. Immunol. **14**(3), 141–153 (2014).
2. D. Du, F. Xu, L. Yu, C. Zhang, X. Lu, H. Yuan, Q. Huang, F. Zhang, H. Bao, L. Jia, X. Wu, X. Zhu, X. Zhang, Z. Zhang, and Z. Chen, "The tight junction protein, occludin, regulates the directional migration of epithelial cells," Dev. Cell **18**(1), 52–63 (2010).
3. R. Weissleder and V. Ntziachristos, "Shedding light onto live molecular targets," Nat. Med. **9**(1), 123–128 (2003).
4. J. M. Jabbour, M. A. Saldua, J. N. Bixler, and K. C. Maitland, "Confocal endomicroscopy: instrumentation and medical applications," Ann. Biomed. Eng. **40**(2), 378–397 (2012).
5. K. L. Turner, S. A. Miller, P. G. Hartwell, N. C. MacDonald, S. H. Strogatz, and S. G. Adams, "Five parametric resonances in a microelectromechanical system," Nature **396**, 149–152 (1998).
6. H. Li, X. Duan, Z. Qiu, Q. Zhou, K. Kurabayashi, K. R. Oldham, and T. D. Wang, "Integrated monolithic 3D MEMS scanner for switchable real time vertical/horizontal cross-sectional imaging," Opt. Express **24**(3), 2145–2155 (2016).
7. F. Laermer and A. Urban, "Challenges, developments and applications of silicon deep reactive ion etching," Microelectron. Eng. **67–68**, 349–355 (2003).
8. A. D. Rakić, "Algorithm for the determination of intrinsic optical constants of metal films: application to aluminum," Appl. Opt. **34**(22), 4755–4767 (1995).
9. T. Hinoi, A. Akyol, B. K. Theisen, D. O. Ferguson, J. K. Greenson, B. O. Williams, K. R. Cho, and E. R. Fearon, "Mouse model of colonic adenoma-carcinoma progression based on somatic Apc inactivation," Cancer Res. **67**(20), 9721–9730 (2007).
10. N. C. Deliolanis, R. Kasmieh, T. Wurdinger, B. A. Tannous, K. Shah, and V. Ntziachristos, "Performance of the red-shifted fluorescent proteins in deep-tissue molecular imaging applications," J. Biomed. Opt. **13**(4), 044008 (2008).
11. J. Zhou, B. P. Joshi, X. Duan, A. Pant, Z. Qiu, R. Kuick, S. R. Owens, and T. D. Wang, "EGFR Overexpressed in Colonic Neoplasia Can be Detected on Wide-Field Endoscopic Imaging," Clin. Transl. Gastroenterol. **6**(7), e101 (2015).
12. L. Liu, E. Wang, X. Zhang, W. Liang, X. Li, and H. Xie, "MEMS-based 3D confocal scanning microendoscope using MEMS scanners for both lateral and axial scan," Sens. Actuators A Phys. **215**(15), 89–95 (2014).
13. B. P. Joshi and T. D. Wang, "Exogenous Molecular Probes for Targeted Imaging in Cancer: Focus on Multi-modal Imaging," Cancers (Basel) **2**(2), 1251–1287 (2010).

#302038 https://doi.org/10.1364/BOE.8.005533
Journal © 2017 Received 10 Jul 2017; revised 31 Oct 2017; accepted 31 Oct 2017; published 13 Nov 2017

Biomedical Optics EXPRESS

14. M. Goetz, A. Ziebart, S. Foersch, M. Vieth, M. J. Waldner, P. Delaney, P. R. Galle, M. F. Neurath, and R. Kiesslich, "In vivo molecular imaging of colorectal cancer with confocal endomicroscopy by targeting epidermal growth factor receptor," Gastroenterology **138**(2), 435–446 (2010).
15. S. Foersch, R. Kiesslich, M. J. Waldner, P. Delaney, P. R. Galle, M. F. Neurath, and M. Goetz, "Molecular imaging of VEGF in gastrointestinal cancer in vivo using confocal laser endomicroscopy," Gut **59**(8), 1046–1055 (2010).
16. C. Fottner, E. Mettler, M. Goetz, E. Schirrmacher, M. Anlauf, D. Strand, R. Schirrmacher, G. Klöppel, P. Delaney, M. Schreckenberger, P. R. Galle, M. F. Neurath, R. Kiesslich, and M. M. Weber, "In vivo molecular imaging of somatostatin receptors in pancreatic islet cells and neuroendocrine tumors by miniaturized confocal laser-scanning fluorescence microscopy," Endocrinology **151**(5), 2179–2188 (2010).
17. A. S. Wellikoff, R. C. Holladay, G. H. Downie, C. S. Chaudoir, L. Brandi, and E. A. Turbat-Herrera, "Comparison of in vivo probe-based confocal laser endomicroscopy with histopathology in lung cancer: A move toward optical biopsy," Respirology **20**(6), 967–974 (2015).
18. A. Meining, E. Frimberger, V. Becker, S. Von Delius, C. H. Von Weyhern, R. M. Schmid, and C. Prinz, "Detection of cholangiocarcinoma in vivo using miniprobe-based confocal fluorescence microscopy," Clin. Gastroenterol. Hepatol. **6**(9), 1057–1060 (2008).
19. V. J. Konda, A. Meining, L. H. Jamil, M. Giovannini, J. H. Hwang, M. B. Wallace, K. J. Chang, U. D. Siddiqui, J. Hart, S. K. Lo, M. D. Saunders, H. R. Aslanian, K. Wroblewski, and I. Waxman, "A pilot study of in vivo identification of pancreatic cystic neoplasms with needle-based confocal laser endomicroscopy under endosonographic guidance," Endoscopy **45**(12), 1006–1013 (2013).
20. P. Kim, E. Chung, H. Yamashita, K. E. Hung, A. Mizoguchi, R. Kucherlapati, D. Fukumura, R. K. Jain, and S. H. Yun, "In vivo wide-area cellular imaging by side-view endomicroscopy," Nat. Methods **7**(4), 303–305 (2010).
21. J. Ahn, K. Choe, T. Wang, Y. Hwang, E. Song, K. H. Kim, and P. Kim, "In vivo longitudinal cellular imaging of small intestine by side-view endomicroscopy," Biomed. Opt. Express **6**(10), 3963–3972 (2015).
22. X. Duan, H. Li, J. Zhou, Q. Zhou, K. R. Oldham, and T. D. Wang, "Visualizing epithelial expression of EGFR in vivo with distal scanning side-viewing confocal endomicroscope," Sci. Rep. **6**, 37315 (2016).
23. E. Laemmel, M. Genet, G. Le Goualher, A. Perchant, J. F. Le Gargasson, and E. Vicaut, "Fibered confocal fluorescence microscopy (Cell-viZio) facilitates extended imaging in the field of microcirculation. A comparison with intravital microscopy," J. Vasc. Res. **41**(5), 400–411 (2004).

1. Introduction

The internal body surfaces of small animals used for research are covered with epithelium [1]. This thin layer of tissue has a depth of ~200 μm, and is the origin of tumor cell proliferation, migration, and invasion. Real-time in vivo imaging with sub-cellular resolution is being developed to monitor cell movement. Individual cells can migrate and proliferate in an arbitrary direction [2]. Thus, optical sections in 3-dimensions are needed for thorough study of cell function and fate. Also, expression patterns of molecular targets can be useful for evaluating new therapies [3]. Biopsies taken for pathological evaluation provide static information at finite time points only, and provide no knowledge of disease progression.

Endomicroscopy is a powerful method of optical sectioning that uses flexible optical fibers [4]. An instrument with proper dimensions and geometry can be used repetitively over time in small animals to track individual cells in vivo. Conventional optics and scanners are large and bulky, and require wide surgical exposure that may introduce significant trauma. Until now, in vivo imaging of cellular behavior in the epithelium has been limited by a lack of instruments that can be easily maneuvered and accurately positioned. Current instruments use front-view optics that collect images in the horizontal plane only. Because firm contact with tissue is required to couple light, this orientation has limited use in small animals. Side-view optics provide greater utility in narrow, confined lumens.

We develop scanners with sufficiently small dimensions to be placed in the post-objective position. In this configuration, the incident beam can pass through the focusing optics on-axis so that a diffraction-limited spot can be scanned with wide angular deflections to achieve a large field-of-view (FOV). Sensitivity to spherical aberrations is minimized. Also, this geometry allows for the instrument to be scaled down in size to millimeter dimensions for either endoscope compatibility or repetitive small animal imaging.

A scanner that translates axially is needed to image with depth and generate 3D images. With post-objective scanning, the focus moves in an oblique rather than either a pure horizontal or vertical direction. Cell movement can be tracked by tracing its path in the

Biomedical Optics EXPRESS

volumetric images. Monolithic designs can reduce scanner dimensions and simplify the packaging strategy for the instrument.

Here, we aim to demonstrate a confocal endomicroscope that uses a fast, monolithic 3-axis scanner located in the post-objective position to collect fluorescence images in 3-dimensions to visualize individual cells in vivo.

2. Imaging system

Fluorescence excitation is provided at λ_{ex} = 561 (iChrome MLE LFG, Toptica Photonics) and 660 nm (660-S, Toptica Photonics), Fig. 1. Visible and NIR excitation is provided to demonstrate the broad use of this instrument. The visible beam (blue) passes through a triple edge dichroic mirror (DM_1, Di01-R442/514/561, Semrock), is reflected at 90° by a static mirror M_1 (PF10-03-G01, Thorlabs), and is focused by lens L_1 (PAF-X-2-A, Thorlabs) into a 2 meter long single mode fiber (SMF, S405-XP, Thorlabs) with 3 µm mode field diameter. The beam exiting the SMF is focused by side-view optics (L_2-L_4), and scanned by the monolithic 3-axis mirror M_2. The NIR beam (red) passes through a second dichroic mirror (DM_2, FF685-Di02-25x36, Semrock). A flip mirror (FM, PF10-03-G01, Thorlabs) is used to switch between the two sources.

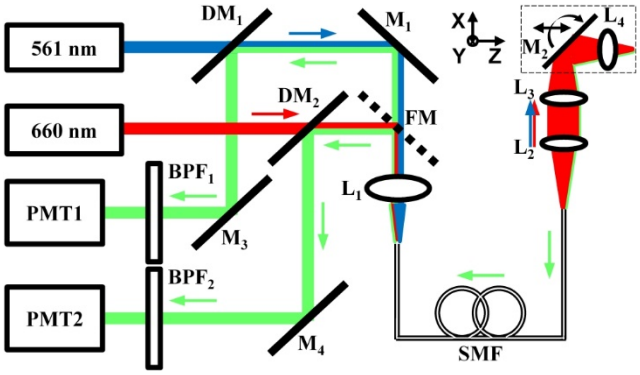

Fig. 1. Schematic of imaging system. Details are provided in text. Key: DM – dichroic mirror, M – mirror, FM – flip mirror, SMF – single mode fiber, L – lens, BPF – band pass filter, PMT – photomultiplier tube.

Fluorescence (green) is collected by the same distal optics (L_2-L_4), descanned by M_2, and focused into the SMF. After transmission through the fiber, fluorescence is collimated by L_1, reflects off either M_1, DM_1 and M_3 or FM, DM_2, and M_4. Photomultiplier tubes (PMT1, H7422-40, Hamamatsu) and (PMT2, H7422-40, Hamamatsu) detects either visible or NIR fluorescence, respectively, that passes through either band pass filter (BPF_1, FF01-485/537/627-25) or (BPF_2, FF01-716/40-25, Semrock). A high-speed current amplifier (59-178, Edmund Optics) boosts the signal, which is digitized by a multi-function data acquisition board (PCI-6115, National Instruments). The board also generates control signals to drive the scanner, and is controlled with custom software (LabVIEW, National Instruments).

3. Design of side-view optics

We performed ray-trace simulations (ZEMAX, ver 13) to design the side-view optics (L_2-L_4). Our goal is to use commercially available optics to achieve near diffraction-limited resolution with the mirror M_2 in the neutral position, FOV ≥700 × 600 µm^2, and vertical depth ≥200 µm. Only lenses with outer diameter ≤3 mm were considered for use in the scaled down instrument. We identified lens L_2 (45-262, Edmund Optics, f = 12 mm, 3 mm OD) to collimate light exiting the SMF, and lens L_3 (45-089, Edmund Optics, f = 6 mm, 3 mm OD, NA = 0.25) to focus the beam. The scan mirror M_2 reflects the beam by 90° into the solid

Biomedical Optics EXPRESS

immersion lens L_4 (65-263, Edmund Optics, f = 2 mm, 1.5 mm OD, NA = 0.375), Fig. 2(a). The side-view optics has an overall NA = 0.38.

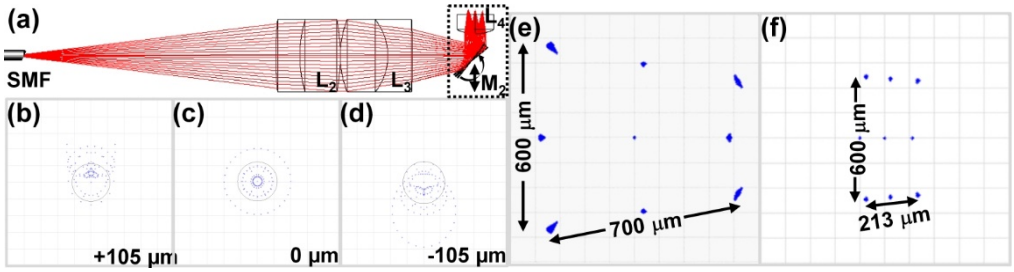

Fig. 2. a) Ray trace diagram shows mirror M_2 located in post-objective position of focusing optics (L_2-L_3). b-d) Simulation results for focal spot size over axial range (+ 105 to −105 µm) of M_2. FOV in e) horizontal and f) projection of vertical plane onto L_4.

The solid immersion lens L_4 functions to minimize spherical aberrations as light passes into tissue and to provide contact. With M_2 at locations + 105, 0 and −105 µm in the Z-axis, the spot sizes of the Airy disks are 1.51, 1.12, and 1.53 µm, respectively, Fig. 2(b)-2(d). Thus, the diffraction limit of 1.19 µm is approached with M_2 at Z = 0 µm.

We also performed ray trace simulations to determine the image FOV. Lateral mirror deflections of ± 10° and ± 8° in the X- and Y-axes, respectively, produce a 700 × 600 µm^2 FOV in the horizontal plane, Fig. 2(e). The combined lateral deflection of ± 8° in the X-axis with axial displacement of ± 105 µm in the Z-axis produced a FOV of 600 × 292 µm^2 in the oblique plane, and is projected onto the horizontal plane with dimensions of 600 × 213 µm^2, Fig. 2(f).

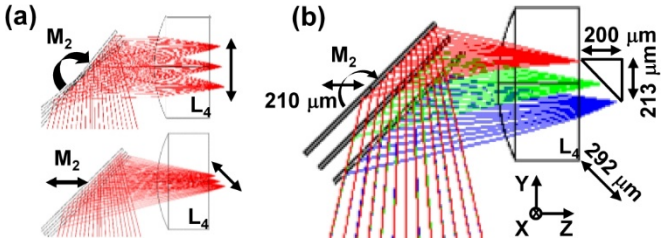

Fig. 3. a) 3-axis scanner provides either lateral or axial motion to direct beam through solid immersion lens (L_4). b) Angular deflection of M_2 results in 213 µm lateral displacement, while axial translation of M_2 produces 200 µm vertical displacement. Combined motion produces 292 µm travel in oblique plane.

When mirror M_2 rotates about the X- and Y- axes, the focus moves laterally, and when M_2 translates in the Z-axis, the focus moves in an oblique direction, Fig. 3(a). The focus is designed to move vertically over depths ranging between + 90 and −110 µm (200 µm total) from the neutral position and laterally from −101 to + 112 µm (213 µm total), Fig. 3(b). The overall dimension traversed by the focus in the oblique plane is 292 µm.

4. Design of monolithic 3-axis scanner

We used ray trace simulations to determine the dimensions of the beam incident on the reflector surface when M_2 translates axially. This result was used to design the geometry of the monolithic 3-axis scanner. The mechanism of actuation is based on parametric resonance where drive signals with frequencies near $2\omega_0/n$ (ω_0 is the natural frequency of each mode, n is an integer ≥1) are used [5]. When M_2 translates from −105 to + 105 µm in the Z-axis, the incident beam forms an ellipse on the reflector surface and traces out an area with dimensions of 1800 and 1200 µm in the major and minor axes, respectively. We used this geometry to determine the reflector geometry, Fig. 4(a).

Biomedical Optics EXPRESS

The reflector is mounted on a gimbal frame that isolates the inner and outer axes to minimizes crosstalk, Fig. 4(b), 4(c). The gimbal is attached to the substrate via multi-beam torsional springs that determine the frequency response of the mirror. The gimbal is also attached to U-shaped suspensions that are designed to either rotate in the Y-axis or displace in the Z-axis out-of-plane when driven at unique frequencies near resonance, Fig. 4(d) [6].

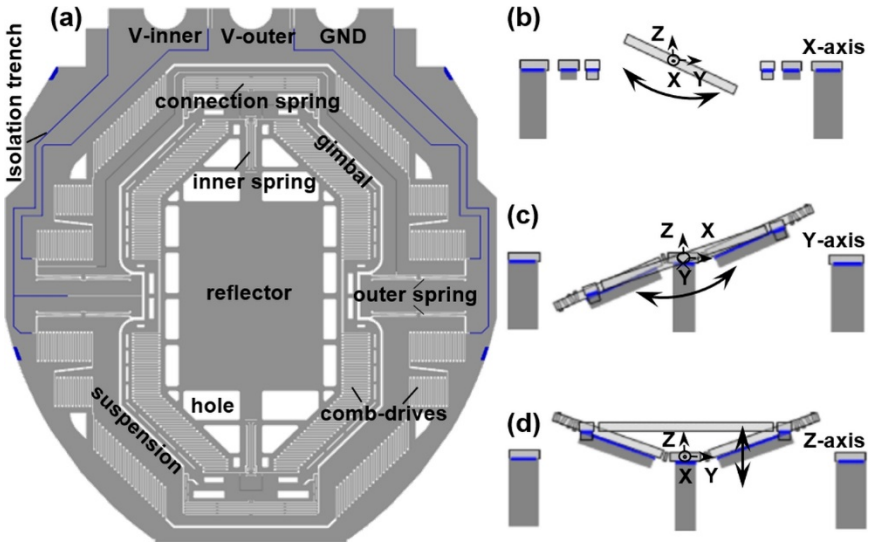

Fig. 4. a) Reflector with dimensions of 1800 and 1200 μm^2 is attached to a gimbal frame driven laterally by actuators coupled to b) inner (X-axis) and c) outer (Y-axis) torsional springs. d) U-shaped suspensions displace the reflector out-of-plane in the Z-axis. Isolation trenches are etched in the device layer to electrically isolate the drive signals between the inner and outer comb-drives.

The scanner was fabricated using a 3 step deep reactive-ion etch (DRIE) process [7]. We used a cutting-free approach to fabricate the scanner with the desired geometry. We introduced a deep cavity in the back side of the silicon-on-insulator (SOI) substrate to provide ample space for the reflector to displace axially while rotating at large deflection angles. We deposited a 70 nm layer of aluminum (Al) film on the reflector surface to achieve >80% reflectivity between 400 and 800 nm [8]. We etched air release holes around the edges of the reflector to minimize air damping effects when sealed in the scanhead.

5. Packaging of endomicroscope

We designed a MEMS chip with 550 μm thickness to mechanically support and electrically connect the scanner. A CAD drawing shows the chip attached to a holder that is used to support the scanner, Fig. 5(a). The lateral chip dimensions are provided, Fig. 5(b). A clearance of about 100 μm was needed to pass the edges of the holder through a stainless-steel tube with ID of 3.8 mm that served as the body of the endomicroscope. We fabricated the holder from M3 crystal, an acrylic based resin with high strength and stiffness, using a 3D printer (ProJet 3500HD MAX, 3DSystems) with 16 μm resolution. A photo of the released 3-axis scanner seated on the chip is shown, Fig. 5(c). We inserted 3 copper (Cu) pins into the chip to serve as electrical contacts. Aluminum (Al) wires (inset) were used to deliver the drive signals, Fig. 5(d). We used glue rather than wire bonds to simplify the assembly process.

Biomedical Optics EXPRESS

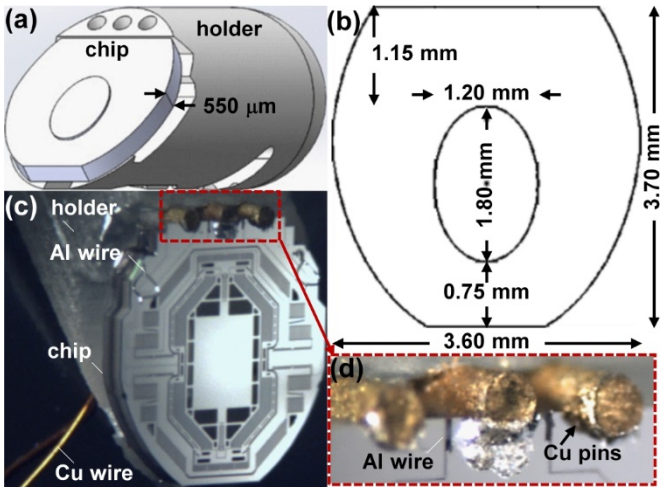

Fig. 5. a) Schematic shows chip used to support monolithic 3-axis scanner attached to holder. b) Lateral chip dimensions. c) Photo of mounted scanner. d) Aluminum (Al) wires are attached to copper (Cu) pins to deliver drive signals.

A schematic shows how the optical fiber, optics, and scanner are assembled in the packaged side-view endomicroscope, Fig. 6(a). The distance between individual optical elements in the scanhead was precisely adjusted using alignment fixtures. We used a laser scan pattern on the flat surface of L_4 to center the image to accurately position M_2. The instrument has a distal diameter of 4.2 mm, Fig. 6(b). The flat surface of L_4 is placed in contact with tissue to collect images. We qualitatively estimated a lateral resolution of ~2 μm (group 7, element 6 in inset) from images collected in the horizontal plane at a working distance of Z = 100 μm from a standard (USAF 1951) resolution target, Fig. 6(c).

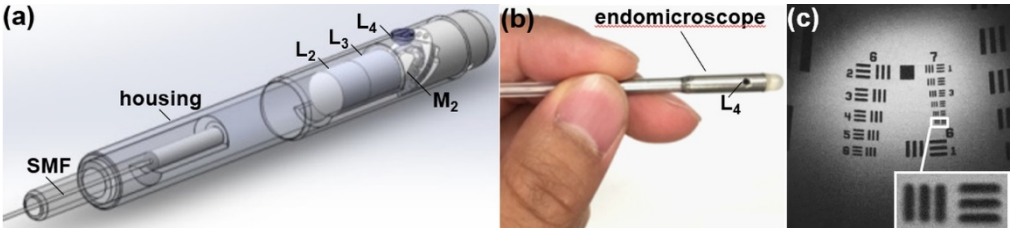

Fig. 6. a) Schematic. CAD drawing shows assembly diagram for packaging of single mode fiber (SMF), stainless steel housing, lenses (L_2-L_4), and scanner (M_2). b) Photo of assembled instrument. c) Reflectance image collected from standard target (USAF 1951) shows lateral resolution of ~2 μm.

6. 3-axis scanner performance

We characterized the lateral and axial response of the MEMS scanner using a position sensing detector and a displacement sensor, respectively. We used either an upsweep (low-to-high) or downsweep (high-to-low) in frequency to drive the device. We applied different sets of drive signals to the scanner to achieve the desired image dimensions and frame rates in the horizontal and oblique planes to collect in vivo and ex vivo images, Table 1.

Biomedical Optics EXPRESS

Table 1. Parameters used to operate monolithic 3axis scanner, including drive frequencies f_X and $f_{Y/Z}$ in the X-, Y-, and Z- axes, show tradeoffs between image FOV and frame rate (Hz).

	imaging plane	frame rate (Hz)	field-of-view (µm2)	field-of-view (pixels)	fX (kHz)	fY/Z (kHz)
in vivo	horizontal	10	600×600	400×400	9.100	1.480
	oblique	10	600×292	500×200	9.120	1.100
ex vivo	horizontal	2	700×600	700×600	9.100	1.484
	horizontal (zoom)	2	80×80	400×400	9.410	1.844

For in vivo imaging, we used a dense Lissajous pattern that repeats itself at 10 frames per second to generate images with dimensions of 400 × 400 pixels with 100% coverage. For ex vivo imaging, a scan pattern at 2 frames per second was used to cover 700 × 600 pixels. We used a downsweep in drive frequency to achieve a maximum lateral mechanical scan angle greater than ± 10° in either the X- or Y-axes, Fig. 7(a), 7(b).

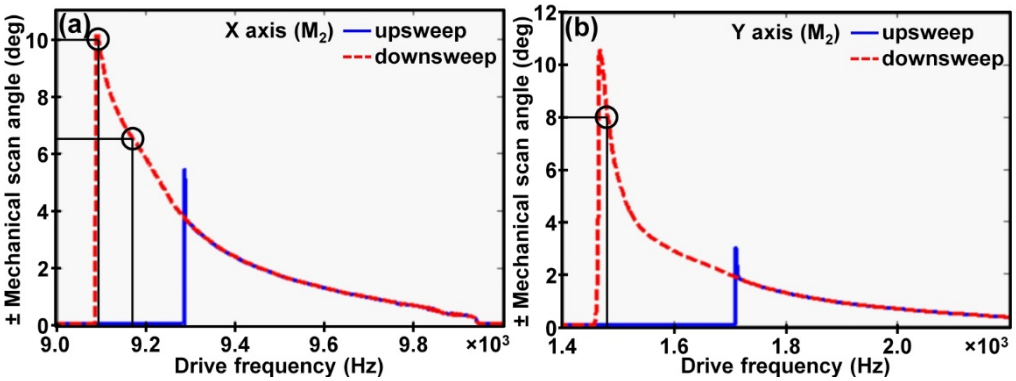

Fig. 7. Drive signals with either an upsweep or downsweep in frequency is used to characterize the scanner response in the a) X- and b) Y-axes.

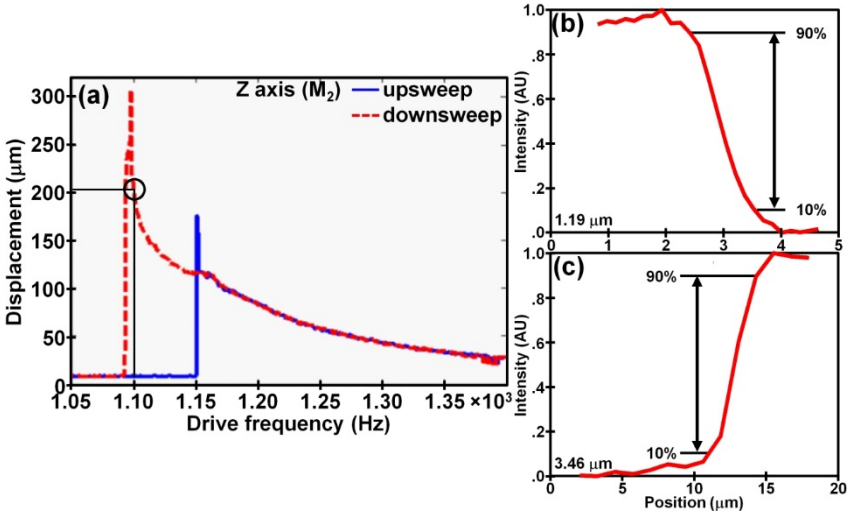

Fig. 8. a) Response of monolithic 3-axis scanner in Z-axes. Resolution of b) 1.19 and c) 3.48 µm was measured in horizontal and oblique plane, respectively, using metric of 10%-90% of maximum intensity from a knife-edge target.

We also used a downsweep to produce the maximum out-of-plane displacement >300 µm in the Z axis, Fig. 8(a). By adjusting the drive frequency to activate either the tilt or piston mode, we can "switch" the scanner to image in either the horizontal or oblique plane. Using a

Biomedical Optics EXPRESS

sine wave at 60 V_{pp}, we drove the X- and Y- axes at f_X = 9.100 and f_Y = 1.480 kHz, respectively, to produce mechanical scan angles of ± 10° and ± 8°, respectively, to achieve a FOV of 600 × 600 μm^2 in the horizontal plane for in vivo imaging. We slightly reduced the FOV to achieve faster imaging at 10 frames per second. We drove the X-axis at f_X = 9.120 kHz with a sine wave at 60 V_{pp} and the Z-axis at f_Z = 1.100 kHz with a square wave at 35% duty cycle and 60 V_{pp} to achieve a FOV of 600 × 292 μm^2 in the oblique plane.

7. Imaging parameters

We measured the lateral resolution quantitatively using the 10%-90% of maximum intensity from a knife-edge target. The resolution in the oblique plane was determined using the same metric. We quantified a resolution of 1.19 and 3.46 μm in the lateral and oblique planes, respectively, Fig. 8(b), 8(c).

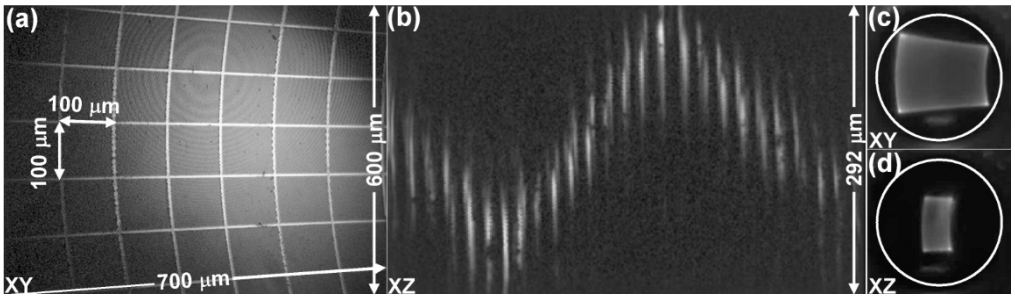

Fig. 9. Reflectance images collected from phantom targets show a) horizontal FOV of 700 × 600 μm^2 and b) vertical depth of 200 μm. Scan patterns in c) horizontal and d) oblique plane projected on flat surface of SIL (L_4) are shown.

We used a 3 × 1 square inch grid distortion target (R1L3S3P, Thorlabs) with 100 × 100 μm^2 squares to evaluate the image FOV, and measured dimensions of 700 × 600 μm^2 in the horizontal plane, Fig. 9(a). The laser scan pattern on the flat surface of the solid immersion lens L_4 can be seen, Fig. 9(b). Imaging depth was evaluated using a phantom consisting of microtrenches etched in a triangular pattern with width and height of 200 μm. We confirmed a vertical depth of 200 μm, Fig. 9(c). The projection of the scan pattern in the oblique plane on L_4 is shown, Fig. 9(d).

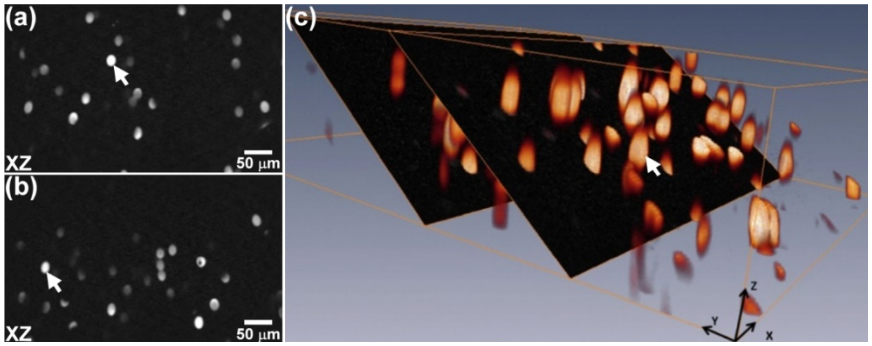

Fig. 10. a,b) Individual optical sections are collected in the oblique plane from embedded 15 μm diameter fluorescent beads (arrows) using λ_{ex} = 660 nm. c) Stack of oblique images is used to construct 3D volumetric image.

We prepared a 3D phantom using 15 μm diameter fluorescent beads (#F-8843, Invitrogen) embedded in UV epoxy (#NOA61, Norland Products Inc). Individual optical sections are collected in the oblique plane using λ_{ex} = 660 nm show individual beads (arrow), Fig. 10(a),(b). A stack of oblique images was combined to construct 3D volumetric images using custom Matlab (MathWorks, Inc) software, Fig. 10(c).

Biomedical Optics EXPRESS

8. Visible imaging

We collected optical sections from colonic epithelium of live animals using visible and NIR excitation to demonstrate the broad use of this instrument. All experimental procedures were performed in compliance with guidelines of the University of Michigan and were conducted with approval by the University Committee on the Use and Care of Animals (UCUCA). We used the genetically engineered CPC;Apc mouse with a Cdx2 promoter to drive a Cre recombinase that sporadically deletes the Apc gene. As a result, adenomas develop spontaneously in the distal colon [9].

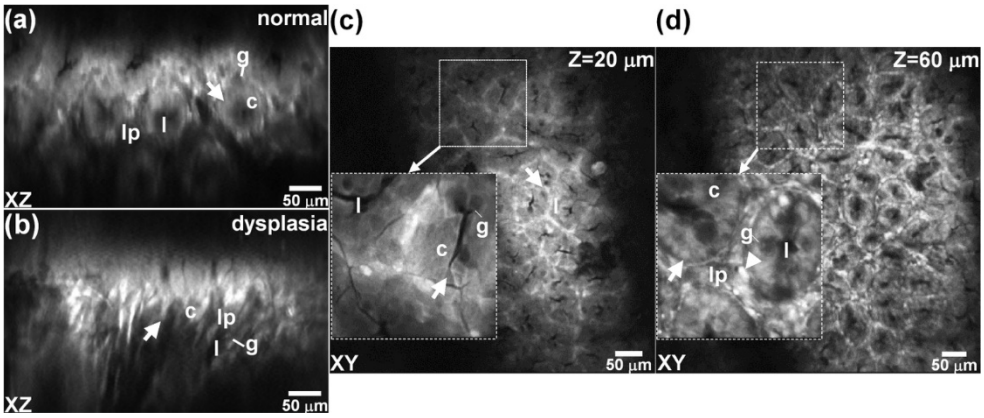

Fig. 11. Using λ_{ex} = 561 nm, fluorescence images collected in vivo in the oblique plane from a) normal and b) dysplastic colonic epithelium from mouse colonic epithelium expressing tdTomato are shown. Images collected ex vivo in horizontal plane at depths of Z = c) 20 and d) 60 μm are shown. Electronically magnified ROIs with dimensions of 80 × 80 μm^2 (inset) clarify individual cells. Key: crypt (arrow), lumen (l), goblet cells (g), cytoplasm (c), inflammatory cells (arrowhead), lamina propria (lp).

The mice were housed in pathogen-free conditions and supplied with water ad libitum under controlled conditions of humidity (50 ± 10%), light (12/12 hour light/dark cycle) and temperature (25°C). During imaging, the mice were anesthetized with 2% isoflurane (Fluriso; MWI Veterinary Supply Co). We used the distance between the endoscope tip and the anus and the clockwise location of the adenoma as landmarks. The angle and extent of insertion were controlled using a translational stage with a rotational fixture to place the optics in direct contact with the lesion. Live video streams were collected at 10 frames per second.

We first used visible excitation at λ_{ex} = 561 nm to collect endogenous fluorescence in vivo from mouse colonic epithelium expressing tdTomato. This fluorescent protein has peak absorbance at ~554 nm [10]. During imaging, we first determined the presence and location of adenomas using a white light wide-field endoscope (27030BA, Karl Storz Veterinary Endoscopy). In the oblique plane, normal crypts appear oval in shape and uniform in size, Fig. 11(a), but dysplastic crypts are elongated in shape and variable in dimension, Fig. 11(b). We reduced the frame rate to 2 per sec for ex vivo imaging, and increased the drive voltage to the scanner to electronically magnify ROIs with an area of 80 × 80 μm^2 (inset) to clarify epithelial features. We validated crypt structures (arrow) containing goblet cells (g) surrounding a central lumen (l) near the epithelial surface in normal colon (Z = 20 μm), Fig. 11(c). Fluorescence is seen uniformly in the cytoplasm (c) of individual colonocytes. At greater depths (Z = 60 μm), we can clearly identify lamina propria (lp) in gaps between individual crypts and occasional inflammatory cells (arrowheads), Fig. 11(d).

Biomedical Optics EXPRESS

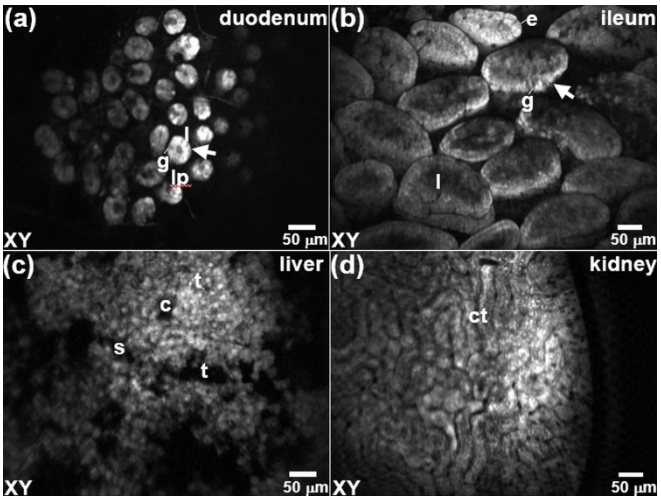

Fig. 12. Fluorescence images are collected ex vivo in the horizontal (XY) plane from a) duodenum, b) ileum, c) liver, and d) kidney to demonstrate the broad applicability of this instrument to identify single cells in other mouse organs. Key: crypt (arrow), goblet cells (g), lumen (l), lamina propria (lp), enterocytes (e), sinusoids (s), central vein (c), portal triads (t), and collecting tubules (ct) in the renal cortex.

We also collected fluorescence images ex vivo from other mouse organs to identify single cells. Individual goblet cells (g) in the duodeunum are seen surrounding a central lumen (l) within crypt (arrow) structures separated by lamina propria (lp), Fig. 12(a). Individual enterocytes (e) and goblet cells (g) in the ileum are seen within the lumen (l) of plica circularis Fig. 12(b). Image of liver lobule shows central vein (arrow) surround by portal triads (t) and perfused by sinusoids (s), Fig. 12(c). Image of kidney shows collecting tubules (ct) in the renal cortex, Fig. 12(d).

9. NIR imaging

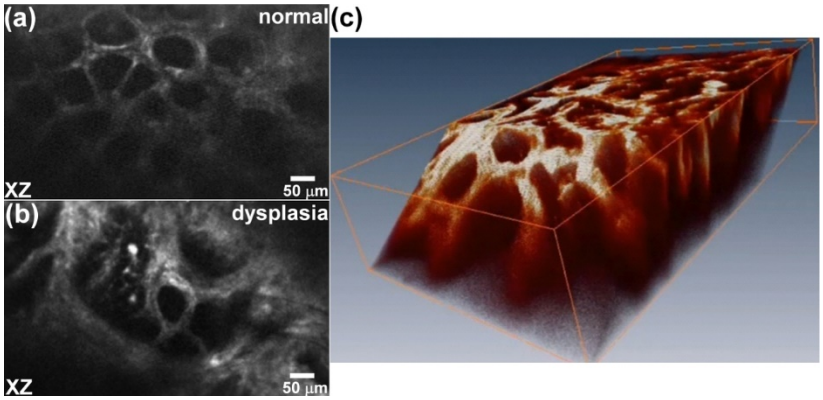

Fig. 13. NIR images of EGFR expression. Fluorescence images are collected ex vivo from mouse colonic epithelium ~2 hours after systemic injection of a Cy5.5-labeled EGFR peptide. Oblique images of a) normal and b) dysplasia. c) A 3D volumetric image is generated from combining a stack of oblique images collected from dysplasia.

We also used NIR excitation at λ_{ex} = 660 nm to detect exogenous contrast from a Cy5.5-labeled peptide with sequence QRHKPRE found to be specific for EGFR [11]. We performed an intra-peritoneal injection of 300 μM of peptide dissolved in 200 μL of PBS via tail vein of CPC;Apc mice. Imaging was performed ex vivo ~2 hour after peptide injection when peak uptake in adenomas was achieved. In the horizontal plane, we visualized minimal staining

Biomedical Optics EXPRESS

from normal colonic epithelium, and found crypts to be circular in shape with uniform dimensions. Dysplasia showed strong staining, and the crypts were irregular in shape and larger in size. In the oblique plane, we saw evenly spaced oval crypts, Fig. 13(a), while dysplastic crypts were distorted in architecture and larger in size, Fig. 13(b). We combined a stack of oblique images from dysplasia to produce a 3D volumetric image, Fig. 13(c).

10. Discussion

Here, we demonstrate a side-view endomicroscope that uses a monolithic 3-axis scanner to generate 3D images and provide optical sections in arbitrary planes. Because of its small size, the device is placed in the post-objective position where focusing can be performed on-axis with minimal spherical aberrations. The scanner produced either optical scan angles over ± 10° to achieve a FOV of 700 × 600 μm^2 in the horizontal plane or large axial displacements to realize vertical depths of 200 μm. Also, this optical configuration allowed for the instrument to be scaled down in size to millimeter dimensions for high maneuverability, accurate positioning, and repetitive imaging in mouse colon. Using commercially available optics, we achieved a resolution of 1.19 and 3.46 μm in the horizontal and oblique plane, respectively. We were able to identify individual cells that express the optical reporter tdTomato in vivo. Also, we visualized the expression level of EGFR, a common molecular target, to demonstrate potential for monitoring therapy. Artifact from respiratory motion, gut peristalsis, and heart beating was mitigated by imaging at 10 frames per second.

The fast 3-axis scanner provides high performance for in vivo imaging in small animal epithelium. We optimized the dimensions of the multi-beam torsional springs so that the gimbal-mounted reflector can be actuated to achieve either wide angular deflections with optical scan angles over ± 10° or large axial displacements ≥300 μm. By tuning the drive frequency to the device, we can activate either the tilt or piston mode of the device to "switch" between imaging planes. As a result, we were able to achieve a FOV of 700 × 600 μm^2 in the horizontal plane that is much greater than what has been achieved by other endomicroscope designs [6]. Also, to our knowledge, this is the first side-view endomicroscope that can collect images in the vertical plane with tissue depths up to 200 μm. Moreover, ROIs can be electronically magnified to highlight individual cells of interest. We achieved stable and repeatable scanning with consistent flipping of imaging planes with no noticeable interruptions or phase shifts.

The scanner was designed with sufficiently small dimensions to be placed in the post-objective position. In this arrangement, the focus moves in both the lateral and axial directions to image in an oblique rather than pure vertical plane, which can be extracted from 3D volumetric images. The excitation beam passes through the focusing optics on-axis so that a diffraction-limited spot can be scanned over the lateral dimensions of the solid immersion lens to minimize effects of spherical aberrations. We achieved sub-cellular resolution in the horizontal and oblique planes, and were able to visualize individual colonocytes, goblet cells, and inflammatory cells from images collected in vivo in mouse colonic epithelium. Also, this geometry allows for the instrument to be scaled down in size to a diameter to 4.2 mm so that repetitive imaging could be performed in mouse colon over time. This feature may allow for investigation of the relationship between cell migration and physiological tissue changes. By comparison, an instrument using a miniature scanner located in the pre-objective position achieved a FOV of only 180 × 180 μm^2 [12].

Confocal endomicroscopy is a minimally invasive method that has sufficient resolution and speed to study epithelial processes in live animals. Other imaging modalities, including X-ray, ultrasound, CT and MRI, provide structural rather than functional information [13]. PET has inadequate resolution to distinguish single cells. We used a side-view geometry to provide high maneuverability for accurate positioning of the optics onto suspicious areas that were first identified with wide-field endoscopy. Animals that express optical reporters can be studied longitudinally to reduce the numbers needed per experiment and improve statistical

Biomedical Optics EXPRESS

power. This instrument can also be used to acquire real time images of molecular expression patterns to evaluate presence of therapeutic targets. Previously, a front-view confocal endomicroscope has been used to evaluate expression levels of EGFR, VEFGR, and somatostatin in animals using exogenous imaging agents [14–16]. Clinical imaging may also be performed in small caliber lumens, including pulmonary bronchioles, biliary tract, and pancreatic duct, that are not accessible with front-view optics [17–19].

Our flexible fiber instrument scans with axial depths exceeding 200 μm that spans the thickness of the epithelium in small animals. This performance represents a significant advance in intra-vital imaging by comparison with other side-view endomicroscopes [20–22]. Previously, a microprobe was developed for wide-area imaging that uses a rigid GRIN lens for focusing and a prism to deflect the beam. Lateral scanning was performed by combining a bulky galvanometer and a rotating polygonal mirror at the proximal end as part of a tabletop system. This optical configuration and scanning strategy does not allow for imaging in the vertical plane. The objective mechanically rotates to produce a wide map of mouse epithelium, and repetitive imaging of colon was demonstrated. The lateral and axial resolution was 1 and 10 μm, respectively, and a FOV of 250 × 250 μm^2 was obtained. This design was adapted for confocal imaging by adding a pinhole in front of the detector. A proximal scanner has been demonstrated that images in horizontal planes only at a fixed working distance of 100 μm.

Front-view endomicroscopes also have limitations in performance and ease of use. A hand-held, confocal probe based on a resonant fiber has demonstrated optical sections in the horizontal plane with depths up to 250 μm. Scanning is performed at the distal end, and a FOV of 475 × 475 μm^2 was achieved with lateral and axial resolution of 0.7 and 7 μm, respectively. In vivo imaging of VEGF was performed in the colon of APC^{min} mice using an Alexa-Fluor 488-labeled antibody specific for VEGF.21 This rigid 5 mm diameter instrument required wide surgical exposure of the abdomen that may elicit an injury response from immune mediators. Also, a flexible instrument with front-view optics based on a fiber bundle has demonstrated optical sections in the horizontal plane at fixed depths ranging between 30 and 100 μm [23]. Scanning is performed at the proximal end with galvos, and a FOV of 160 × 120 μm^2 with lateral and axial resolution of 2.5 and 20 μm, respectively, was achieved. The fiber bundle limits image resolution, and separate miniprobes are needed to image in different horizontal planes.

The performance of this 3-axis side-view endomicroscope can be further improved. In vivo imaging speeds can potentially be increased to 20 frames per second by tuning the dimensions of the torsional springs attached to the inner and outer axes and U-shaped suspension of the gimbal. Instrument dimensions can be further scaled down in size with use of optics that are custom designed and fabricated, and resolution can be improved. Greater vertical displacements can be achieved by mitigating air damping effects with use of a vacuum to reduce the ambient pressure in the scanhead. With further development, we may be able to visualize epithelial cell migration and differentiation in the vertical plane over time and elucidate fundamental mechanisms of cell function and fate. This real time optical imaging technology may be used to study signals that control important molecular pathways, including immune function, tissue regeneration, and host response, and may substantially accelerate development and evaluation of novel therapies.

Funding

National Institutes of Health (NIH) R01 EB020644 (KRO), R01 CA200007 (TDW), and Mary L. Petrovich.

Acknowledgments

We thank Kathy Cho and Rong Wu for use of the genetically engineered tdTomato mouse.

Biomedical Optics EXPRESS

Disclosures

XD, HL, and TDW are inventors on patent application filed by the University of Michigan on the technology presented.